

Structural and Optical Properties of Nanocrystalline $\text{Sn}_{0.93}\text{Mn}_{0.07}\text{O}_2$: Role of Oxygen Vacancies

Naseem Ahmad^{1,b)}, Shakeel Khan^{1,a)}, Mohd Mohsin Nizam Ansari¹ and Richa Bhargava¹

¹Department of Applied Physics, Z. H. College of Engineering and Technology, Aligarh Muslim University, Aligarh UP 202002

^{a)}Corresponding author: skhanapd@gmail.com

^{b)}naseemmultani786@gmail.com

Abstract. In the present work, structural and optical properties of $\text{Sn}_{0.93}\text{Mn}_{0.07}\text{O}_2$ have been studied comprehensively. The tetragonal phase of the sample and the functional groups were demonstrated by XRD and FTIR spectroscopy respectively. The average crystallite size was found to be 19.5 calculated from the Scherer equation and 21.5 nm from Williamson Hall analysis. Optical band gap and Urbach energy of the sample estimated are at 3.78 eV and 0.752 eV respectively. The existence of the defects like oxygen vacancies is verified by photoluminescence spectroscopy and its influence on the structural and optical properties of $\text{Sn}_{0.93}\text{Mn}_{0.07}\text{O}_2$ is also discussed.

Keywords: Optical band gap, Urbach tail, oxygen vacancies, lattice strain, SnO_2 .

INTRODUCTION

Oxygen vacancies like defects have been a typical source of disparity of physical and chemical properties of materials, especially in the metal oxide semiconductors. These often form unintentionally at the surface of metal oxide semiconductors during the synthesis process and are very common to play a significant role in the applications of (photo, heterogeneous) catalysis and biomedical engineering¹. In the case of SnO_2 , which is a wide band gap metal oxide semiconductor, the defects like oxygen vacancy liberate electrons to conduction band disclosing the co-existence of the conductivity and optical transparency without increasing interband absorptions². It is obvious, oxygen vacancies not only influence the conductivity and optical transparency of SnO_2 but also play an important role to produce a ferromagnetic order in the materials. For example, in Co-doped SnO_2 , oxygen vacancies along with Co ions induced the ferromagnetic coupling by enhancing the magnetic moment of Co ions³. Instead of oxygen vacancies, doping of the impurity elements such as transition metal has a considerable impact on the characteristics of tin oxide nanoparticles. By now, a lot of work regarding the modification of the structural, electrical, optical and magnetic properties of SnO_2 by using impurity doping have been reported⁴⁻⁷.

The main focus of this paper is to explore the optical (band gap, Urbach tail) and structural properties (crystalline phase, crystallite size, and lattice strain) of 7% Mn-doped SnO_2 synthesized via precipitation route and to find out the effect of the oxygen vacancies on the aforementioned properties. The detailed structural investigation was carried out using X-Ray diffraction measurement, and the stretching and bending vibrations of functional groups present in the material were depicted by Fourier transforms infrared spectroscopy. The study of optical parameters was carried out by UV-Vis reflectance spectroscopy. Emission (photoluminescence) spectroscopy provides an excessive platform for understanding the defects induced photon emission.

SAMPLE PREPARATION AND CHARACTERIZATIONS

AR grade extra pure $\text{SnCl}_2 \cdot 2\text{H}_2\text{O}$ and $\text{MnCl}_4 \cdot 4\text{H}_2\text{O}$ were taken in a stoichiometric ratio to prepare $\text{Sn}_{0.93}\text{Mn}_{0.07}\text{O}_2$ sample by precipitation method with the calcination temperature of 600 °C. Synthesized powder sample was then characterized by X-ray diffraction measurement in the diffraction angle (2θ) range 20-80° using Rigaku Miniflex 2nd X-ray diffractometer and Fourier transform infrared spectroscopy by means of Perkin Elmer spectrum 2 FTIR spectrometer in the wavenumber range 400-4000 cm^{-1} for structural studies.

Optical properties were investigated by UV-Visible reflectance spectroscopy using Perkin Elmer Lambda 950 UV-Vis/NIR spectrometer under the wavelength range 200 nm to 800 nm and emission spectroscopy by means of Perkin Elmer LS 55 fluorescent spectrophotometer.

RESULTS AND DISCUSSION

Structural properties

Tetragonal rutile phase of the as-prepared $\text{Sn}_{0.93}\text{Mn}_{0.07}\text{O}_2$ sample was confirmed by x-ray diffraction (XRD) measurement with diffraction angle (2θ) 20° to 80° and scanning rate of 4 degree per minute which is displayed in figure 1. It is observed that 7% Mn substitution does not alter the tetragonal phase of the sample as there is no additional impurity phase or peak of MnO or MnO₂ spotted in XRD spectrum (figure 1) of the prepared sample. The clear appearance, sharpness and high intensity of the XRD peaks reveal the good crystallinity of the as-synthesized sample. In order to get further information about the synthesized sample, Fourier transform infrared (FTIR) spectrum of $\text{Sn}_{0.93}\text{Mn}_{0.07}\text{O}_2$ was recorded to disclose the bonding vibrations of the functional groups such that metal oxygen bond, C=O bond, OH bond, etc. present in the material. FTIR spectrum of $\text{Sn}_{0.93}\text{Mn}_{0.07}\text{O}_2$, demonstrated in figure 1, discloses the four clearly appeared significant peaks at 625, 1629, 2332, 3425 cm^{-1} . The broad peak around 625 cm^{-1} is due to antisymmetric stretching of Sn-O-Sn (surface bridging oxide), O-Sn-O and (Sn, Mn)-O stretching and bending vibrations^{8,9}. The peaks 1629 cm^{-1} and 3430 cm^{-1} corresponds to OH stretching vibration which is due to the absorbed water molecule at the surface of the sample¹⁰. The small peak near 2332 cm^{-1} may be due to absorption of the Infrared radiation by the hydrogen bond formed in the material⁵.

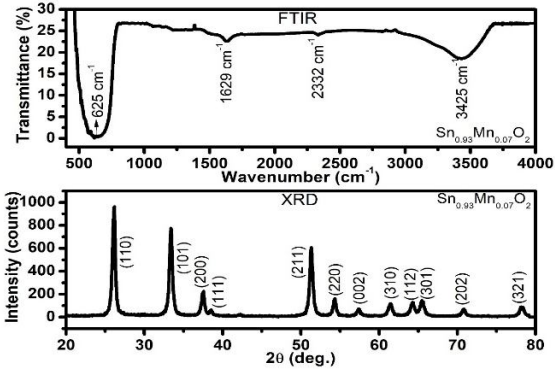


Figure-1: XRD and FTIR spectra of $\text{Sn}_{0.93}\text{Mn}_{0.07}\text{O}_2$

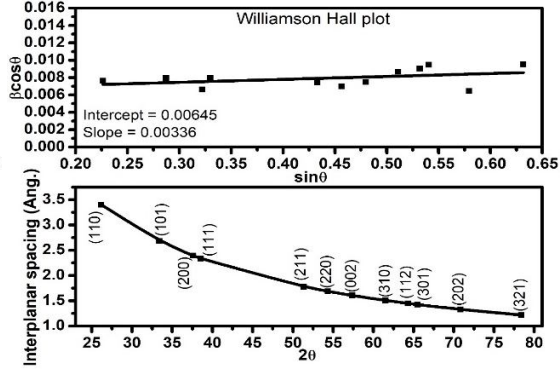


Figure-2: Interplanar spacing and Williamson Hall plot for $\text{Sn}_{0.93}\text{Mn}_{0.07}\text{O}_2$

The average crystallite size of the sample was determined by two methods: Scherer equation and Williamson Hall analysis. Where Scherer equation for particle size calculation can be written as

$$D = \frac{0.9\lambda}{\beta \cos\theta} \quad (1)$$

According to Williamson and Hall, the broadening of XRD peaks β_{hkl} is the outcome of two type broadenings¹¹.

$$\beta_{hkl} = \beta_o + \beta_s \quad (2)$$

Where β_o and β_s corresponds to the size and strain broadenings respectively and may be written as

$$\beta_{hkl} = \frac{k\lambda}{D \cos\theta} + 4\varepsilon_s \tan\theta \quad (3)$$

$$\beta_{hkl} \cos\theta = \frac{k\lambda}{D} + 4\varepsilon_s \sin\theta \quad (4)$$

Here k is shape factor (~ 0.9 for spherical crystallites), $\lambda = 1.54056 \text{ \AA}$ is the wavelength of the X-ray used, D denotes the average crystallite size of the material, θ is the diffraction angle and ε_s represents the lattice strain in the material. The slope and the intercept of linearly fitted WH plot give the value of lattice strain and average crystallite size respectively.

The average crystallite size of $\text{Sn}_{0.93}\text{Mn}_{0.07}\text{O}_2$ sample is found to 19.5 nm and 21.5 nm calculated from the Scherer equation and Williamson Hall analysis respectively. The difference between the magnitude of the crystallite size derived from the two techniques may assign to the contribution of the lattice strain which is

found to 8.4×10^{-4} approximately¹². Since the lattice strain leads to expansion or contraction in the lattice, the incorporation of the Mn content in the host SnO₂ may be the reason of more stretching or expanding of the lattice parameters due to the different ionic radius of Sn⁴⁺ ions (69 pm) and Mn³⁺/Mn⁴⁺ ions (65 pm/53 pm)¹³. The contraction in the lattice may also be the consequence of oxygen vacancies. It is also observed that the interplanar spacing (d) corresponds to different diffraction planes, as shown in figure 2, decrease with increasing diffraction angles.

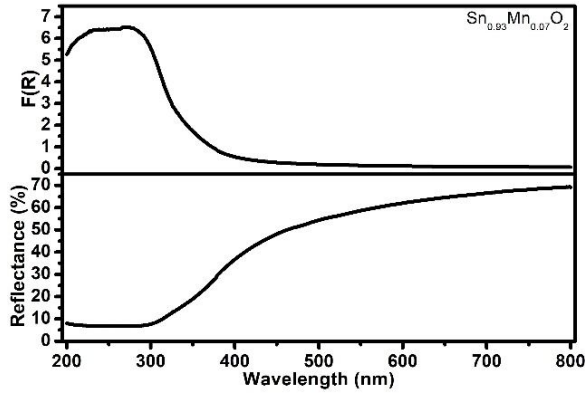


Figure-3: Reflectance and absorbance spectra of Sn_{0.93}Mn_{0.07}O₂

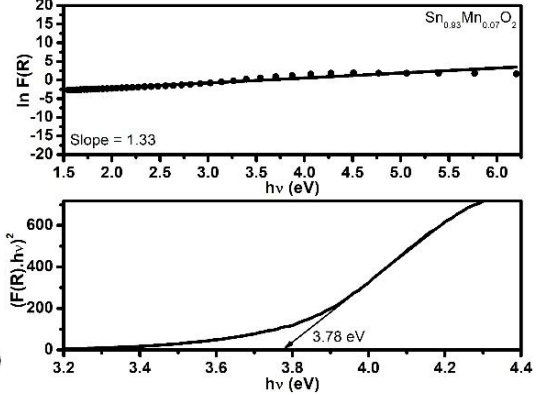


Figure-4: Urbach and Tauc plot for Sn_{0.93}Mn_{0.07}O₂

Optical properties

In order to estimate the optical band gap and Urbach energy of the as-prepared sample reflectance spectroscopy is used. The reflectance spectra and the corresponding Kubelka Munk function (absorbance) in the wavelength range 200-800 nm have been shown in figure 3. Optical band gap describes the energy gap between the topmost point of the valence band and the lowest point of the conduction band, i.e. the energy height of the forbidden region. Besides, the band tail width or Urbach tail generally expressed as the energy structure originated near the edges of the absorption band (CB and VB) due to the electron-phonon interaction. It is also described as a tail of energy bands due to localized states related with the disordering in the sample⁴. Since the oxygen vacancies (arisen to maintain charge imbalance in Sn_{0.93}Mn_{0.07}O₂) and other defects (impurity doping and other point defects) take significant participation in disordering of the crystal lattice, the band tail (Urbach tail) may assign to this defects induced disordering. Further, the oxygen vacancies may produce defect (donor) levels or thin band of donor levels below the conduction band edge in the forbidden region of energy bands and hence often leads to the reduced energy band gap of the material⁹. It is clear from figure 3, Mn-doped SnO₂ sample exhibits high reflectivity towards the visible region of the electromagnetic spectrum whereas absorbance (KM function) of the material is quite high in the ultraviolet region. Since the optical band gap of tin oxide material belongs to the ultraviolet region, the high absorption in the ultraviolet region is due to the direct band to band transition of the electrons.

Kubelka Munk function $F(R)$ which is the function of reflectance and directly proportional to absorbance can be written as $F(R) = \frac{(1-R)^2}{2R}$. The optical band gap E_g of the sample is calculated from Tauc relationship: $F(R)hv = A(hv - E_g)^n$. And Urbach energy or Urbach tail (band tail width) has been estimated using the expression: $\alpha = \alpha_0 \exp(E/E_u)$. Where $E = hv$ is the energy of incident electromagnetic radiation, α is absorption coefficient ($\propto F(R)$), R is the reflectance, E_u is Urbach tail (Urbach energy), A is constant and $n=1/2$ for direct band gap semiconductors. The extrapolation of the linear part of the Tauc plot at energy axis gives the energy band of the sample which is found to 3.78 eV and the reciprocal of the slope of the linear fit of the Urbach plot ($\ln R$ vs hv) provide Urbach tail or Urbach energy which is equal to 0.752 eV.

Photoluminescence spectroscopy (emission spectroscopy) is a valuable tool for the investigation of the oxygen vacancy like defects produced in the crystalline material. Photoluminescence spectrum of the as-synthesized sample has been shown in figure 5. The excitation energy to record the emission spectrum of the sample was equivalent to the optical band gap calculated by reflectance spectroscopy. On the other hand, the deconvolution of the PL spectrum precisely discloses the three major emission peaks in which two are highly intense at 413 nm and 433 nm and remaining broad one is shoulder peak at 462 nm. All the three major peaks appeared in PL spectrum cannot belong to direct band to band transition as the equivalent energies of the wavelength of the peaks (3.00 eV, 2.86 eV center 2.68 eV respectively) are not equal to the estimated optical band gap energy (3.78 eV). The emission peak appeared at 413 nm may assign to the band to band transition mediated

by oxygen vacancies and the second one at 433 nm attributed to the luminescent center formed due to dangling and tin interstitials present in the crystal lattice⁶. The broad shoulder peak centered at 462 nm may ascribe to two electron trapping at oxygen vacancy's sites¹⁴.

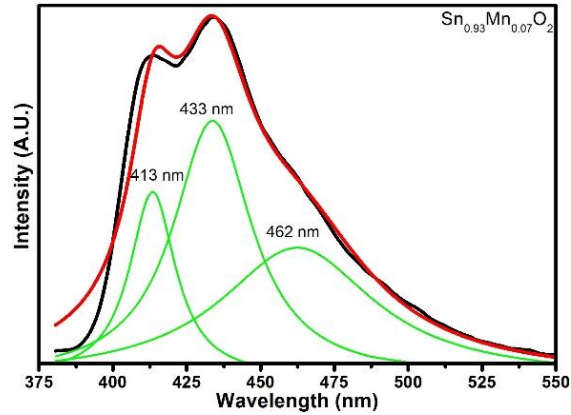


Figure-5 Deconvolution of the emissionspectrum of $\text{Sn}_{0.93}\text{Mn}_{0.07}\text{O}_2$

CONCLUSION

Role of oxygen vacancies in the structural and optical properties of $\text{Sn}_{0.93}\text{Mn}_{0.07}\text{O}_2$ sample has been explored successfully. The presence of the oxygen vacancies and other defects was confirmed by photoluminescence spectroscopy which in turn affect the band tail width and the band gap of the sample. It is concluded that oxygen vacancies not only influence the optical properties of the sample but have an impact on the crystalline parameters, i.e. it may cause the contraction and hence become an effective source of lattice strain and small crystallites in the material.

BIBLIOGRAPHY

1. L.Z. Liu, X.L. Wu, F. Gao, J.C. Shen, T.H. Li, and P.K. Chu, *Solid State Commun.* **151**, 811 (2011).
2. C. Kilic and A. Zunger, *Phys. Rev. Lett.* **88**, 955011 (2002).
3. H. Wang, Y. Yan, Y.S. Mohammed, X. Du, K. Li, and H. Jin, *J. Magn. Mater.* **321**, 3114 (2009).
4. N. Ahmad, S. Khan, and M.M.N. Ansari, *Ceram. Int.* **44**, 15972 (2018).
5. N. Ahmad, S. Khan, M. Mohsin, and N. Ansari, *Mater. Res. Express* **5**, 035045 (2018).
6. N. Ahmad and S. Khan, *J. Alloys Compd.* **720**, 502 (2017).
7. N. Ahmad, S. Khan, M. Mohsin, N. Ansari, R. Bhargava, M.M.N. Ansari, and R. Bhargava, in *AIP Conf. Proc.* (2018), p. 050007.
8. F.E.G.J. Mazloom, *Appl. Phys. A Mater. Sci. Process.* **108**, 693 (2012).
9. P. Chetri and A. Choudhury, *Phys. E Low-Dimensional Syst. Nanostructures* **47**, 257 (2013).
10. M. Parthivarman, K. Vallalperuman, S. Sathishkumar, M. Durairaj, and K. Thavamani, *J. Mater. Sci. Mater. Electron.* **25**, 730 (2014).
11. V.D. Mote, Y. Purushotham, and B.N. Dole, *J. Theor. Appl. Phys.* **6**, 6 (2012).
12. N. Ahmad, S. Khan, and M.M.N. Ansari, *Mater. Res. Express* **5**, 035045 (2018).
13. R.D. Shannon, *Acta Crystallogr. Sect. A* **32**, 751 (1976).
14. D. Li, H. Haneda, N.K. Labhsetwar, S. Hishita, and N. Ohashi, *Chem. Phys. Lett.* **401**, 579 (2005).